Nature of Excited States and Relaxation Mechanisms in C-Phycocyanin

Jordan M. Womick and Andrew M. Moran*

Department of Chemistry, The University of North Carolina at Chapel Hill, Chapel Hill, North Carolina 27599

Received: August 21, 2009; Revised Manuscript Received: October 15, 2009

The electronic structure and photoinduced relaxation dynamics of the cyanobacterial light harvesting protein, C-Phycocyanin (CPC), are examined using transient grating and two-dimensional (2D) photon echo spectroscopies possessing sub-20 fs time resolution. In combination with linear absorption and fluorescence measurements, these time-resolved experiments are used to constrain the parameters of a Frenkel exciton Hamiltonian. Particular emphasis is placed on elucidating the nature of excited states involving the α84 and β84 phycocyanobilin pigment dimers of CPC. This paper obtains new experimental evidence suggesting that electronic relaxation proceeds by way of incoherent energy transfer between the α84 and β84 pigment sites (i.e., the weak coupling limit of energy transfer). Transient absorption anisotropies simulated in the weak coupling limit agree well with measurements, whereas signals computed in an exciton basis possess short-lived (electronic) coherent components not present in the experimental data. In addition, 2D photon echo spectra for CPC show no sign of the interfering nonlinearities predicted by a theoretical model to be characteristic of exciton formation. Another important new observation is that the sub-100 fs dynamics in the transient absorption anisotropy are dominated by an impulsively excited hydrogen out-of-plane wagging mode similar to those observed in phytochrome and retinal. Detection of this 795 cm^{-1} coherence is of particular interest because our recent study of a closely related protein, Allophycocyanin (APC), assigns a similar coordinate as a promoting mode enabling ultrafast internal conversion. Together, the experiments conducted for APC and CPC suggest that interactions between the pigments and environment are the key to understanding why electronic relaxation in CPC is more than three times slower than APC despite the nearly identical geometries of the pigment dimers. Most important in reaching this conclusion is the present finding that relaxation of the 2D photon echo line shapes of CPC is approximately two times faster than that measured for APC. Overall, the present results underscore the ability of phycobiliproteins to control light harvesting dynamics through solvation and variation in the conformations of open-chain tetrapyrrole chromophores.

I. Introduction

Essential to the understanding of photoinduced relaxation in multichromophore systems is the composition of excited states.[1−4] When wave functions delocalize among multiple chromophores, transitions between exciton states proceed through solvent fluctuations and vibronic internal conversion channels. By contrast, incoherent energy transfer dynamics take hold for systems in which excited state wave functions are localized to the individual molecules comprising the complex.[5−8] Frenkel exciton models applied to photosynthetic proteins, molecular aggregates, and organic crystals show that (delocalized) exciton wave functions originate in interactions between molecular transition moments.[1−4,9−11] The appropriate view of electronic structure is governed by the relative sizes of these intermolecular couplings and system−bath interaction strengths, where the latter tend to localize wave functions to the individual pigment sites.[12,13] The delineation of relaxation mechanisms is not always clear in photosynthetic proteins because the interactions between pigments separated by less than a few nanometers are generally comparable to the amplitudes of environment-induced energy level fluctuations.[14−17] Understanding the nature of excited states in such systems generally relies on the application of advanced theory and experiments.

In this paper, the nature of the excited states and relaxation mechanisms of C-Phycocyanin (CPC) are investigated using femtosecond laser spectroscopies. As shown in Figure 1, the structure of CPC consists of nine phycocyanobilin pigments arranged about a 3-fold axis of symmetry.[18−20] The structure is

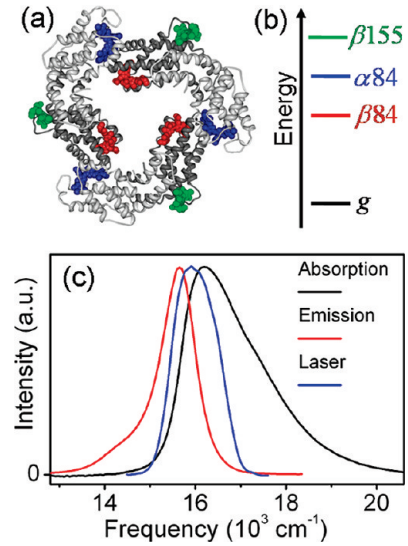

Figure 1. (a) Structure of CPC trimer in which red, blue, and green, respectively, represent the β84, α84, and β155 pigments. (b) Energy level diagram for three pigments. (c) Absorption (black) and fluorescence emission (red) spectra for CPC overlaid with the spectrum of laser pulses used for most of the measurements.

* Corresponding author. E-mail: ammoran@email.unc.edu.

10.1021/jp908093x CCC: $40.75

considered a "trimer" composed of three α (light gray) and three β (dark gray) monomer subunits. Upon trimer formation, the α84 and β84 pigments of adjacent monomer units come into close contact. Excited state delocalization in these pairs of α84 and β84 pigments (i.e., dimers) is the central issue addressed in this work. The α84 and β84 pigments within a particular dimer are separated by only 2.1 nm, whereas the separation between all other pairs of pigments in CPC is >5 nm. Close proximity of pigments within the dimer opens the possibility that intermolecular interactions give rise to exciton formation. In fact, several investigations find evidence of exciton formation in the α84-β84 pigments of a closely related protein, Allophycocyanin (APC), in which the geometry of the dimer is quite similar to that of CPC.[21−25] Experiments conducted in this paper closely examine the interplay between intermolecular couplings and the thermal fluctuations of the environment that compete to localize electronic wave functions. These results are discussed in the context of our recent study of APC.[26] Together, these investigations provide insight into how phycobiliproteins configure their pigments and use environment-induced fluctuations to optimize the efficiency of the phycobilisome antenna.

Electronic relaxation dynamics of CPC have been investigated using spectroscopies that measure anisotropy in either transient absorption or fluorescence emission.[27−30] Although these anisotropy techniques provide similar information, different conclusions have been reached by various authors regarding the nature of relaxation mechanisms (i.e., incoherent energy transfer versus interexciton population decay). One aspect of the dynamics for which there is broad agreement is the presence of a subpicosecond nonradiative transition involving the α84-β84 pigment dimers, which is over 50 times faster than the electronic relaxation processes associated with any other pair of pigments. Much of the present understanding of CPC photophysics is owed to Sauer and co-workers who carefully examined both monomers and trimers using a variety of theoretical and experimental methods.[28,29] It was concluded that the time scale of the transition involving the α84-β84 dimer is well-described with Förster theory. Zhang et al. interpreted fluorescence upconversion measurements using an exciton model but acknowledged that heterogeneity in the molecular site energies, which were unknown at the time, could motivate a description of electronic relaxation based on Förster energy transfer.[31] Gillbro et al. applied transient absorption anisotropy measurements to CPC and assigned a 0.5 ps decay component to Förster energy transfer between the α84 and β84 pigments.[27] The Förster model was deemed appropriate because the spectroscopic line widths of CPC are larger than the estimated 112 cm^{-1} intermolecular coupling in the dimer. By contrast, the transient absorption anisotropy measurements of Riter et al. assigned a 35 fs time constant to internal conversion between exciton states.[30] The present paper agrees with Riter et al. that the sub-100 fs dynamics in the anisotropy are particularly important for elucidating the electronic relaxation mechanisms of CPC. Our transient absorption anisotropy measurements provide new information on these sub-100 fs dynamics with a 7.5-fold improvement in time resolution.

Theoretical and experimental advances occurring in the past decade allow CPC to be examined with improved time resolution and sensitivity. First, the time resolution available in ultrafast spectroscopies has substantially improved because of advances in nonlinear optics.[32−34] The generation of sub-20 fs pulses is now routine in the region of the visible spectrum where CPC absorbs light. Technical developments have also made possible the application of a variety of nonlinear spectroscopies analogous to multidimensional NMR techniques.[35−44] For example, two-dimensional photon echo spectra correlate photoexcited and relaxed states without the compromise in time and frequency resolution inherent to conventional pump−probe techniques.[45−50] In addition, the "cross peaks" resolved in these 2D spectra are particularly sensitive to exciton formation.[51−54] Here we leverage these technical advances for improved physical insight into the electronic structure of CPC.

The present investigation of CPC complements our recent study of APC in which transient grating and two-dimensional photon echo signals were used to constrain the parameters of a Frenkel exciton Hamiltonian.[26] We found that energy gaps at the β84 and α84 sites of APC were, respectively, 15 300 and 16 060 cm^{-1} with an intermolecular coupling of −163 cm^{-1}. This basis of nondegenerate pigments gives rise to excitons that are 96% localized to the individual pigments comprising the dimer. Nonetheless, unambiguous signatures of exciton formation were found in transient absorption anisotropy and photon echo signals. For example, excited state absorption between delocalized single and double exciton states causes the transient absorption anisotropy to increase with the signal emission frequency. Further support for exciton formation in APC derives from the observation of cross peaks in photon echo spectra. In addition, nuclear coherences observed in transient absorption anisotropy signals enabled assignment of the dominant relaxation channel to an 800 cm^{-1} promoting a mode representing a hydrogen out-of-plane wagging vibration similar to those found in phytochrome and retinal.[55−58] Overall, the results suggest that APC uses delocalized electronic states to enhance electronic relaxation rates and rapidly configure itself for efficient energy transfer to the reaction center.

II. Experiment

C-Phycocyanin (CPC), isolated from *Spirulina*, was purchased from Prozyme as a suspension in 60% ammonium sulfate. Spectroscopic measurements used solutions of CPC in 5 mM potassium phosphate buffer at pH 7.0. All experiments were performed within 12 h of solution preparation. Optical experiments circulated the solutions at a rate of 4 mL/s in a flow system using a peristaltic pump with reservoir of 10 mL. The flow rate was set at the maximum value for which turbulence in the flow cell did not appreciably degrade the signal-to-noise ratio. The absorbance of the solution was 0.15 at 16 200 cm^{-1} in a 0.5 mm path length flow cell. Absorbance spectra were measured before and after experiments to confirm the absence of sample degradation.

The one-color transient grating (TG) and photon echo (PE) experiments in this paper use the same equipment and procedures described elsewhere.[59−61] Briefly, the TG and PE experiments use a diffractive optic-based interferometer similar to those reported in several earlier publications.[39,40,62−65] The apparatus applies four pulses in a boxcars (square) laser beam geometry. Pulses with durations of 17 fs and energies of 5 nJ are focused to 120 um spot size at the sample for a fluence of 1.4×10^{14} photons/cm^2. Increasing the pulse energies by a factor of 4 has no effect on the measured dynamics. Signals are detected by spectral interferometry using a back-illuminated CCD array (Princeton Instruments PIXIS 100B) mounted on a 0.3 m spectrograph. Integration times are 100−200 ms. Signals are processed using a Fourier transform algorithm.[35,66,67]

Anisotropies compare tensor elements for real (absorptive) TG signal components measured in immediate succession, where each tensor element represents an average of 15 scans of the optical delay line (25 min total data acquisition time). The

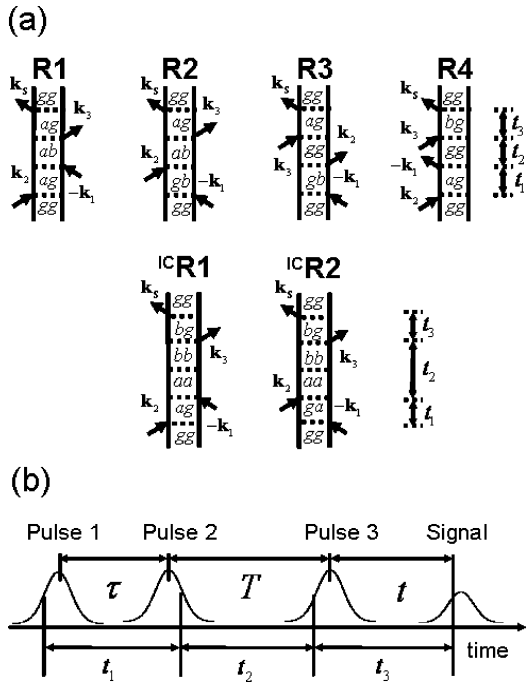

Figure 2. (a) Feynman diagrams for dominant terms in the transient grating and photon echo spectroscopies in this paper. R1, R2, R3, and R4 are restricted to terms in which $a = b$ when the zeroeth order Hamiltonian of eq 1 does not include (weak) intermolecular interactions. The superscript IC used in the bottom row denotes incoherent exciton transport. Terms in the nonlinear response function corresponding to these diagrams are presented in Appendix B. (b) Pulse sequence used for TG and PE spectroscopies. The delays, τ and T, are experimentally controlled. Intervals between field−matter interactions are given by t_1, t_2, and t_3.

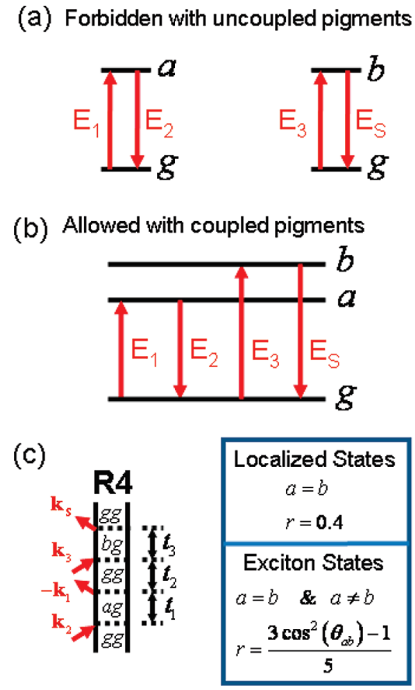

Figure 3. (a) Sequences with pairs of interactions on pigments uncoupled in the zeroeth-order Hamiltonian, $H_{Sys}^{(0)}$, are forbidden. (b) Pairs of interactions with separate resonances are allowed in the exciton basis. (c) Field−matter interaction sequence expressed for the R4 diagram. Anisotropies depend on relative transition dipole orientations only in the (coupled) exciton basis.

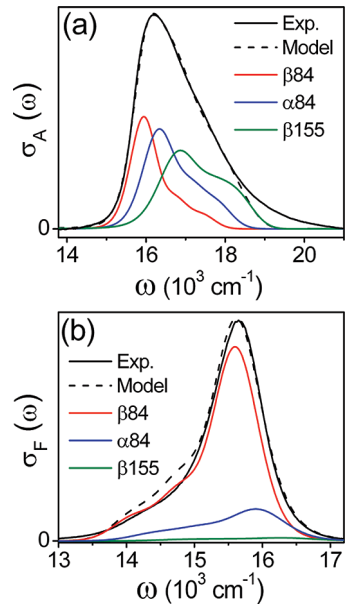

Figure 4. (a) Experimental (black solid) and theoretical (black dashed) linear absorption spectra. Also shown are the line shapes of the β84 (red), α84 (blue), and β155 (green) pigments. (b) Same as (a) for the fluorescence spectrum. The same color scheme is used in Figure 1a.

experiments were repeated several times and suggest that this procedure yields an error of approximately ±0.03 in the anisotropy. The photon echo spectra presented here are performed under the magic angle polarization condition. Rephasing and nonrephasing signals are superposed to obtain absorptive line shapes.[46,48,68] Scans of photon echo spectra at a series of population times are repeated 10 times and averaged for a total data acquisition time of 5 h.

Phase angles of TG and PE signals are defined by reference to the pure buffer solution, which is taken to possess a fully dispersive (imaginary) signal phase because it is transparent to visible light. TG signal fields are first measured with the pure buffer. Calibration of the TG signal phase for CPC is achieved by exchanging the sample reservoir for the CPC solution without moving the flow cell. The PE signal phase is then readily obtained using the projection slice theorem of Fourier transforms.[36] That is, two-dimensional PE signals are integrated over the ω_τ dimension (i.e., Fourier transform of τ delay shown in Figure 2), and the phase of this projection is adjusted for agreement with the TG signal phase. Earlier investigations successfully use this same phasing procedure.[69,70]

The two-color TG measurements presented in Figure 5 use an E_1 and E_2 pulse-pair and an E_3 pulse (see Figure 2) derived from separate optical parametric amplifiers. The spectrum of the E_3 "probe" pulse spans the 500−750 nm range, and we are unable to fully compensate for the dispersion over this broad bandwidth using a prism compressor. The frequency-dependent time overlap of E_3 with the compressed E_1 and E_2 pulse-pair is taken into account numerically using a procedure already well-established for conventional two-pulse transient absorption spectroscopy with a continuum probe.[71] TG signals obtained with the transparent buffer solution are used as a reference to numerically correct the dependence of "time-zero" on the signal emission frequency. We obtain a full-width half-maximum instrument response of <60 fs at signal emission frequencies of 14 500−18 500 cm^{-1} using a prism compressor configured to minimize dispersion at 16 800 cm^{-1}. The Supporting Information presents an example showing TG signals for the buffer with and without this numerical correction. This procedure applies

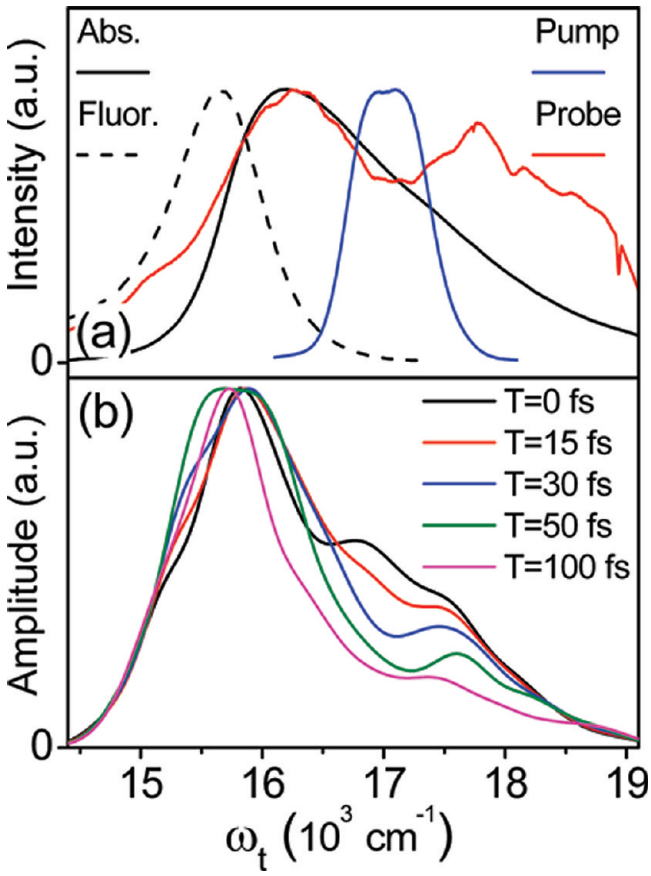

Figure 5. (a) Pump (blue) and probe (red) spectra overlaid on absorption and fluorescence spectra of CPC. (b) Absolute value of transient grating signal fields measured at the pump−probe delay times given in the legend. Signal amplitudes are normalized.

only to the data presented in Figure 5. All other experiments in this paper use laser pulses with time−bandwidth products less than 0.52.

III. Theoretical Model for C-Phycocyanin

IIIA. Parameterization of the Hamiltonian. The site energies and interpigment couplings in CPC have been examined with comprehensive studies of monomers, trimers, and mutant proteins.[28,29] Our parametrization of the system Hamiltonian is guided by these earlier investigations. In addition, spectroscopic line widths and Franck−Condon factors are obtained with consideration of the present measurements. Here, it is necessary to consider a basis of only the three pigments, α84, β84, and β155, because the measurements examine dynamics on a short time scale (<10 ps) for which electronic relaxation occurs only within the α84-β84 dimers. Here the α84 and β84 pigments refer to the closely spaced (2.1 nm) dimers of adjacent peptide units (see Section I). It is irrelevant with which peptide unit β155 is taken to be associated because it transfers energy to other pigments at a rate slow compared to the time scale for which signals are measured and simulated.

Under the assumption of localized electronic states, the zeroeth-order Hamiltonian of the system simply sums over the three pigment sites as

$$H_{\mathrm{Sys}}^{(0)} = \sum_{a}^{3} E_a |a\rangle\langle a| \qquad (1)$$

TABLE 1: Parameters of the Spectroscopic Model

parameter	value	parameter	value
[a] E_a (β84)	15890 cm^{-1}	[b] F_a^{00} (β84)	0.69
[a] E_a (α84)	16240 cm^{-1}	[b] F_a^{00} (α84)	0.52
[a] E_a (β155)	16640 cm^{-1}	[b] F_a^{00} (β155)	0.37
Δ_{aa} (β84)	510 cm^{-1}	$F_{a\nu}^{01}$ ($\nu = 1$, β84)	0.17
Δ_{aa} (α84)	600 cm^{-1}	$F_{a\nu}^{01}$ ($\nu = 1$, α84)	0.21
Δ_{aa} (β155)	700 cm^{-1}	$F_{a\nu}^{01}$ ($\nu = 1$, β155)	0.18
$\lvert\mu_{ga}\rvert$ (β84)	6.5 D	$F_{a\nu}^{01}$ ($\nu = 2$, β84)	0.08
$\lvert\mu_{ga}\rvert$ (α84)	6.5 D	$F_{a\nu}^{01}$ ($\nu = 2$, α84)	0.13
$\lvert\mu_{ga}\rvert$ (β155)	5.4 D	$F_{a\nu}^{01}$ ($\nu = 2$, β155)	0.18
κ_a (all pigments)	0.2	ω_ν ($\nu = 1$)	800 cm^{-1}
k_ν^{-1} (all ν)	10 fs	ω_ν ($\nu = 2$)	1500 cm^{-1}

[a] Energy gap of pigment in eq 1.

where E_a is the energy gap of pigment a (i.e., α84, β84, or β155). This paper regards the intermolecular interactions neglected in eq 1 as weak perturbations inducing incoherent energy transfer between pigment sites.[5−8,14] Because $H_{\mathrm{Sys}}^{(0)}$ is diagonal in the local basis, the energy levels and transition dipoles entering the optical response function are independent of intermolecular couplings. Throughout this paper, we will refer to eq 1 as the zeroeth-order Hamiltonian to emphasize that intermolecular interactions influence spectroscopic signals only through their promotion of incoherent energy transfer; the applied fields interact with localized electronic states.

The time scale and magnitude of environment-induced fluctuations in E_a are described with Λ_{aa}^{-1} and Δ_{aa}, respectively. Spectroscopic line broadening is modeled with a single overdamped Brownian oscillator coordinate in the high-temperature limit

$$g'_{ab}(t) = g'_{ba}(t) = \frac{1}{\kappa_a^2}\left(1 - i\frac{\kappa_a \Delta_{ab}}{2k_{\mathrm{B}}T}\right)[\exp(-\Lambda_{ab}|t|) + \Lambda_{ab}t - 1] \qquad (2)$$

where the symmetrized line broadening function is defined as $g_{ab}(t) \equiv g'_{ab}(t) + g'_{ba}(t)$ and $\kappa_a = \Lambda_{ad}/\Delta_{aa}$.[2,10,72] The optical response functions assume that all vibronic transitions for a pair of electronic states, a and b, share the same $g_{ab}(t)$ function. Essentially, this treatment says that environment-induced fluctuations particular to vibrational coordinates are negligible compared to fluctuations of the electronic energy levels. The parameters of eqs 1 and 2 are given in Table 1. Note that no transformation of eq 2 is necessary because the states of the individual pigments are eigenstates of $H_{\mathrm{Sys}}^{(0)}$. We assume a 60° angle between transition dipoles for the α84 and β84 pigments. This angle is consistent with the present measurements and also within the 52°−65° range suggested by earlier spectroscopic investigations.[27,29]

IIIB. Computation of Spectroscopic Signals. Modern methods for computing spectroscopic signals of photosynthetic proteins and molecular aggregates can be found in recent literature.[2−4,7,73] The model used here is a modified version of that presented in Sections 5.1 and 5.2 of ref 74 where line broadening and exciton transport are described with a cumulant expansion of Gaussian fluctuations. In our recent study of APC, quantized nuclear modes were added to the model of ref 74 to account for vibronic coupling. Here we model experiments using a similar approach with one important difference: signal contributions requiring the inclusion of intermolecular interactions in the zeroeth-order Hamiltonian, $H_{\mathrm{Sys}}^{(0)}$, are neglected. It will be shown below that the transient absorption anisotropy is particularly sensitive to the composition of $H_{\mathrm{Sys}}^{(0)}$.

Figure 2 presents Feynman diagrams representing all terms in the nonlinear response function. Sensitivity of the optical

response to exciton formation centers on the two dummy indices, a and b, involved in the summations of the R1, R2, R3, and R4 terms. Recognizing which terms are forbidden and allowed in these summations is the key to distinguishing exciton electronic structure from states localized to the individual pigments. Specifically, we suggest a rule that terms in which $a \neq b$ must be neglected when intermolecular couplings are not part of $H_{\mathrm{Sys}}^{(0)}$ (see eq 1). Under this condition, intermolecular interactions influence the optical response only through the $^{\mathrm{IC}}$R1 and $^{\mathrm{IC}}$R2 terms by promoting incoherent energy transfer between pigment sites.[5−8] Alternatively, with intermediate and/or strong intermolecular interactions, the couplings are taken into account at zeroeth-order. The Hamiltonian must then be transformed into the exciton basis, and the nonlinear response does not restrict the R1, R2, R3, and R4 summations to terms in which $a = b$.[2,4,10,74]

Figure 3 further explains the type of nonlinearity neglected under the zeroeth-order assumption of uncoupled pigments (eq 1). The key point is that, in the absence of zeroeth-order intermolecular coupling, the R4 nonlinearity can be generated only when all four field−matter interactions occur with the same molecule. Terms in which pairs of interactions occur with the transition dipoles of different pigments cannot contribute because, in essence, these sites do not share the same ground state. By contrast, coherent "cross terms" in which $a \neq b$ contribute when pigment coupling gives rise to exciton electronic structure. Thus, signatures of electronic relaxation mechanisms in the R1, R2, R3, and R4 nonlinearities are quite well-defined. Pigment complexes undergoing Förster energy transfer restrict summations to terms in which $a = b$, whereas systems relaxing by internal conversion between exciton states have unrestricted summations (i.e., $a \neq b$ is allowed).

The $^{\mathrm{IC}}$R1 and $^{\mathrm{IC}}$R2 terms represent incoherent nonradiative transitions between electronic states. These terms are particularly important for interpreting dynamics in transient absorption anisotropy experiments examining weakly coupled pigments because the first two field−matter interactions occur with different transition dipoles than the final two. The anisotropy obtained by summing the $^{\mathrm{IC}}$R1 and $^{\mathrm{IC}}$R2 terms is equal to 0.4 at $t_2 = 0$ and decays to an asymptotic value determined by the relative orientations of the μ_{ga} and μ_{gb} dipoles. These are the only terms in Figure 2 for which summations over $a \neq b$ are allowed with the zeroeth-order Hamiltonian of eq 1. In this limit, the anisotropy obtained by summing over the R1, R2, R3, and R4 terms is equal to 0.4 at all pulse delays.

The nonlinear polarization is computed by convoluting the response function with the applied electric fields as

$$\begin{aligned} P^{(3)}(t) = & \int_0^\infty \mathrm{d}t_1 \int_0^\infty \mathrm{d}t_2 \int_0^\infty \mathrm{d}t_3 [R_1(t_1,t_2,t_3) \\ & + R_4(t_1,t_2,t_3) + {}^{\mathrm{IC}}R_1(t_1,t_2,t_3)] \\ & \times E_3(t-t_3) E_1^*(t-t_3-t_2) E_2(t-t_3-t_2-t_1) \\ & + [R_2(t_1,t_2,t_3) + R_3(t_1,t_2,t_3) + {}^{\mathrm{IC}}R_2(t_1,t_2,t_3)] \\ & \times E_3(t-t_3)\, E_2(t-t_3-t_2) E_1^*(t-t_3-t_2-t_1) \end{aligned} \tag{3}$$

Transient grating and photon echo signals are related to $P^{(3)}(t)$ under perfect phase-matching conditions by

$$E_S(t) = \frac{i2\pi l\omega_t}{n(\omega_t)c} P^{(3)}(t) \tag{4}$$

where $n(\omega_t)$ is the refractive index; l is the sample thickness; and c is the speed of light. Expressions for all terms in the response function are given in Appendix B.

IV. Results and Discussion

IVA. Linear Absorption and Fluorescence Spectra. The linear absorption spectrum is decomposed into transitions at the three pigment sites in Figure 4a, where calculations are performed with the formulas in Appendix A. The site energies are blue-shifted by about 190−390 cm^{-1} compared to the values obtained by studies of monomers and a mutant protein.[28,29] The origin of this blue-shift could be associated with geometry changes induced by trimer formation. It is interesting that our recent investigation of a closely related phycobiliprotein, APC, found a 760 cm^{-1} gap between the transition energies of the two pigments comprising the dimer,[26] whereas that of CPC is only 350 cm^{-1}. X-ray crystal structures for APC and CPC suggest that the energy gaps may be influenced by a difference in pigment conformations.[18−20,75] The fluorescence spectrum shown in Figure 4b is also used to constrain the parameters of the Hamiltonian given in Table 1. The site energies, line widths, and Franck−Condon factors of the α84 and β84 pigments are well-determined by the fit of the fluorescence line shape. By contrast, the line widths and Franck−Condon factors of the β155 pigment are not as well-constrained because β155 contributes very little to the steady state fluorescence spectrum. In any case, uncertainties associated with the β155 pigment do not impact the conclusions of this paper because our experiments and model calculations use laser spectra that overlap little with the absorption spectrum of β155.

IVB. Dynamics of Solvation and Vibrational Cooling. Nuclear relaxation in both CPC and its α-subunit have been examined using hole-burning spectroscopies employing 80 fs pump pulses and continuum probe pulses.[30,76] Red-shifting of the signal spectrum was observed on the 50 fs time scale, whereas line broadening occurred with a time constant of 200 fs. Figure 5 presents transient grating signals aimed at uncovering nuclear relaxation dynamics with improved time-resolution (i.e., <60 fs fwhm instrument response over full probe bandwidth). Solvation dynamics cause significant sub-100 fs red-shifting of the signal spectrum with a concomitant decrease in signal amplitude occurring in the 16 500−18 000 cm^{-1} frequency range. The absence of dynamic line broadening in the measured signal spectrum is explained by the initiation of broad nuclear wavepackets. That is, the present 20 fs pump pulses degrade (frequency) resolution of the transient line broadening dynamics observed in the earlier "hole-burning" experiments.[30,76]

Both intramolecular vibrational energy redistribution (IVR) and solvation likely contribute to the red-shift observed in Figure 5. The solvation time scales are computed as $\Lambda_a^{-1} = 1/\kappa_a\Delta_{aa}$, where time constants of 327, 278, and 238 fs are found for β84, α84, and β155 using the parameters of Table 1, respectively. These calculated solvation time constants are about 5 times slower than the measured dynamics. It may be that the red-shift in the signal spectrum mainly reflects IVR. Another explanation is that this discrepancy reflects a shortcoming of the Brownian oscillator model. Indeed, modern computational solvation models have established the importance of explicitly treating intermolecular interactions in liquids (e.g., electrostatic coupling, hydrogen bonding).[77−82] The important point is that these data prove CPC to be well-configured for fast nuclear relaxation through a combination of IVR and solvation. The X-ray crystal structure indicates substantial access of water to the pockets in which the pigments are bound.[18−20] The ability of water to undergo fast structural reorganization is consistent with the sub-100 fs time scale of the dynamics.[50,83−85]

IVC. Transient Absorption Anisotropy. The transient absorption anisotropy presented in Figure 6 is obtained using

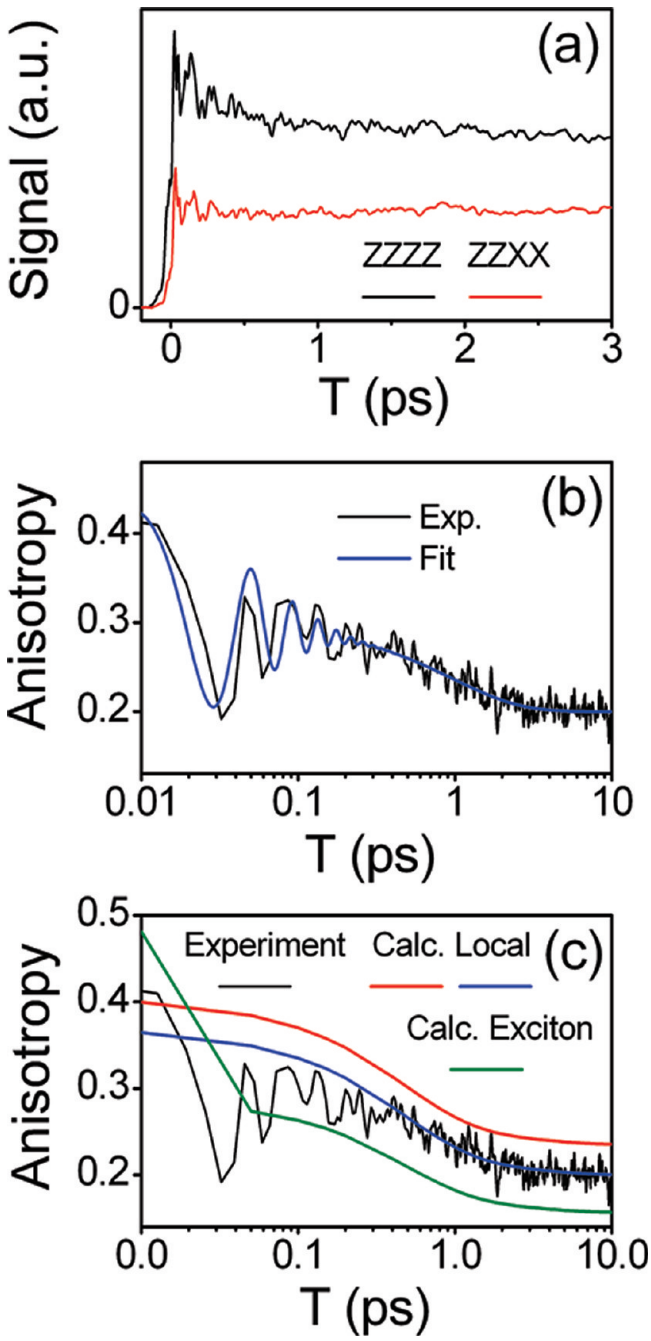

Figure 6. (a) Real part of transient grating signal field measured at $\omega_t = 15\,625$ cm^{-1} with ZZZZ (black) and ZZXX (red) polarization conditions. (b) Anisotropy computed using tensor elements in panel (a) and fit (blue, see Table 2). (c) Anisotropy calculated using parameters in Table 1 (red) and equations in Appendix B where R1, R2, R3, and R4 are restricted to terms in which $a = b$ (i.e., a local basis); the blue line subtracts 0.035 from the red line. The green line assumes exciton formation and computes the anisotropy without restricting the summations of R1, R2, R3, and R4 terms (i.e., $a \neq b$ is allowed).

the real (absorptive) part of the transient grating signal field measured for ZZZZ and ZZXX tensor elements. This representation is equivalent to that found with a conventional pump−probe laser beam geometry.[69] In Figure 6b, the decay profiles are fit with an exponential and damped sinusoidal component for which parameters are given in Table 2. The 970 fs exponential decay represents incoherent energy transfer between the α84 and β84 pigments. The broadband pulses used here excite both the α84 and β84 pigments in roughly equal

TABLE 2: Fits to Anisotropy Measurements Shown in Figure 6

[a]parameter	value
r_0	0.2
r_1	0.1
r_2	0.15
τ_1	970 fs
τ_2	60 fs
ω	795 cm^{-1}
φ	5.0 rad

[a] Fit to equation $r(T) = r_0 + r_1 \exp(-T/\tau_1) + r_2 \cos(\omega T + \varphi)\exp(-T/\tau_2)$.

proportions judging by the overlap of the laser spectrum with the absorption line shapes of the individual pigments (see Figures 1 and 4). The energy gap between the excited states is 350 cm^{-1}. Therefore, significant energy transfer occurs in both directions with the ratio of 5.26 governed by detailed balance. The 970 fs time constant measured here is slower than the time constants found in two earlier measurements for CPC where values of 500 and 690 fs were obtained.[27,30] We believe this difference in measured time constants reflects selective excitation of the α84 pigment in the earlier studies, where pulses with higher frequencies and narrower bandwidths were employed.

The experimental signal possesses a coherent component with a 795 cm^{-1} frequency, which we assign to a hydrogen out-of-plane (HOOP) wagging mode analogous to those observed in retinal polyenes. This assignment is based on comprehensive resonance Raman studies of a related bilin chromophore, phytochrome, which has a structure similar to phycocyanobilin.[55−58] Transient absorption anisotropies measured for the phycobiliprotein APC also exhibit coherences at 800 cm^{-1} reflecting a HOOP vibration.[26] We assigned this coordinate as the promoting mode responsible for ultrafast internal conversion in APC.[26] Appearance of this mode in the transient absorption anisotropy underscores its asymmetric nature.[86]

In Figure 6c, model calculations consistent with the zeroeth-order Hamiltonian in eq 1 sum over R1, R2, R3, and R4 with the restriction that $a = b$. The calculation predicts initial and asymptotic values of the anisotropy of 0.4 and 0.235, respectively. Differences between experiment and calculation are particularly apparent in that the measured r_0 and r_1 components do not sum to 0.4 at $T = 0$ despite the model's prediction that they should. We attribute this discrepancy to a broadband excited state absorption (ESA) nonlinearity localized on the individual pigment. That is, the model calculation obtains an initial anisotropy of 0.4 under the assumption that each pigment is a two-level system, whereas ESA reduces the measured anisotropy because the "pump" and "probe" pulses can then interact with transition dipoles possessing different orientations. This interpretation is supported by transient absorption experiments for the isolated α subunit of CPC, which observed ESA in this frequency range.[76] We presently do not have enough information to accurately parametrize the line shapes of the excited state resonances. However, the contribution of ESA does not weaken the arguments regarding the electronic structure of CPC put forth in this paper. The 970 fs time constant is obtained with or without ESA because the nonlinearity is localized to the pigment site. In other words, ESA essentially produces an "offset" in the magnitude of the anisotropy. To emphasize this point, Figure 6c subtracts 0.035 from the calculated anisotropy to show that the shape of the exponential decay is well-captured by the model with the zeroeth-order Hamiltonian of eq 1.

This paper's primary conclusion of localized electronic states in the α84-β84 dimer is further supported by computing the

anisotropy in an exciton basis where "cross terms" in which $a \neq b$ enter R1, R2, R3, and R4. The anisotropy then has an initial value of 0.48 and an asymptotic value of 0.16 (Figure 6c). This calculated decay profile clearly disagrees with the electronic relaxation dynamics measured at $T < 100$ fs because the calculated R1 and R2 terms evolve as short-lived excited state coherences when $a \neq b$. The failure of the calculation to describe the anisotropy at long times is ascribed to the R3 and R4 ground state bleach terms, which are essentially independent of T. On the basis of the measurements and calculations in this section, we conclude that CPC does not possess exciton electronic structure. We view this comparison of experiment and theory as an important illustration of the power of transient absorption anisotropy for elucidating electronic structure.[87−90] Spectroscopic signatures of these coherent "cross terms" are unambiguous and clearly distinguish fundamentally different models of electronic structure.

The interpretation of localized electronic states reached in this section conflicts with that of Riter et al. who also employed femtosecond transient absorption anisotropy measurements in an investigation of CPC.[30] The present apparatus leverages technical developments occurring in the past decade for a 7.5-fold improvement in time resolution. The time resolution is quite important because it enables assignment of the sub-100 fs dynamics in the anisotropy to an impulsively excited vibration. The measured anisotropy is clearly distinct from the monotonic decay predicted with the response function appropriate for delocalized excited states (green line in Figure 6c). We attribute the vibration's 60 fs dephasing rate to heterogeneity in the ground state (i.e., Franck−Condon) geometry; the photoexcited nuclear coherence dephases quickly in T because the nonlinear polarization radiates as a sum over many incommensurate vibrational frequencies. It should be acknowledged that we do not yet have conclusive evidence that ESA nonlinearities localized at the pigment sites are responsible for the fact that the measured r_0 and r_1 components do not sum to 0.4 at $T = 0$. An alternative viewpoint would see this as a signature of exciton delocalization. However, we believe that the present experiments and analysis argue against this interpretation.

IVD. Impulsively Excited Vibrations. Figure 7 Fourier transforms recurrences in a transient absorption measurement to obtain a spectrum of impulsively excited vibrations. The spectrum in Figure 7 is similar to that measured for APC, where significant amplitude is measured near 250, 600, and 800 cm^{-1}.[91] It should be noted that dominance of the low-frequency part of the spectrum reflects, in part, the finite time resolution of the experiment. The fact that the coherent signal components at 250 and 600 cm^{-1} are not observed in the anisotropy suggests that these resonances represent nuclear motion imposing little distortion of the phycocyanobilin structural symmetry. Resonance Raman investigations of a related chromophore, phytochrome, indicate that resonances at 530 and 635 cm^{-1} involve a mixture of hydrogen out-of-plane (HOOP) wagging and twisting of the methine bridge, whereas HOOP motion dominates the 810 cm^{-1} mode (see Section IVC).[55] The mode near 250 cm^{-1} was not assigned by earlier resonance Raman studies. Because of its low frequency, we propose that it represents twisting the methine bridges (i.e., inter-ring torsion).

IVE. Photon Echo Spectroscopy. The photon echo (PE) signals in this section further test our interpretation that the excited states of CPC are localized to the individual pigments. Figure 8 presents PE spectra measured from $T = 0$ to 120 fs. At $T = 0$ fs, elongation of the spectrum with respect to the diagonal, $\omega_\tau = \omega_t$, represents correlation in the pumped, ω_τ, and probed, ω_t, transition frequencies.[4,36,46,48] The asymmetric

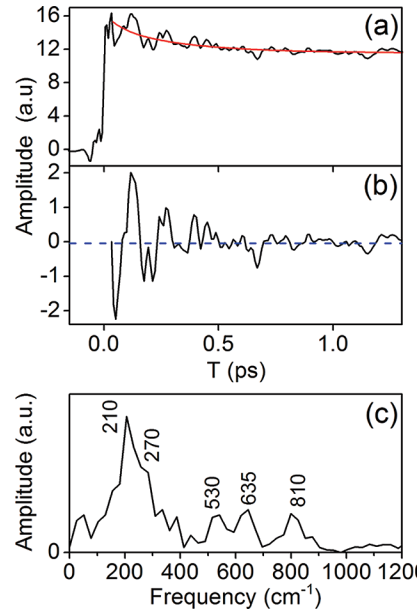

Figure 7. (a) Real part of transient grating signal field measured with 17 fs pump and probe pulses centered at 15 900 cm^{-1}. (b) Nuclear coherences are isolated by subtracting a decaying exponential function (red) from the data in panel (a). (c) Absolute value of Fourier transform of signals in panel (b). The noise level in (c) is approximately 15% of the peak amplitude at 635 cm^{-1}.

peak shape enables separation of the homogeneous and inhomogeneous contributions to the line widths; the 490 cm^{-1} antidiagonal width is the homogeneous contribution. Elongation of the line shape fully relaxes by $T = 30$ fs, which is about 20−30 fs faster than relaxation of the PE spectrum for APC.[26] In addition, a 175 cm^{-1} red-shift in the PE peak maximum occurs on the same time scale as dynamics in the peak shape. The time scale is consistent with the red-shift observed in the transient grating (TG) signals shown in Figure 5 where the dynamics at $T < 50$ fs dominate relaxation of the signal spectrum. Changes in the PE spectra from $T = 50$ to 120 fs mainly involve a decrease in signal amplitude at $\omega_\tau = 16\,100$ cm^{-1}, $\omega_t = 16\,300$ cm^{-1}. Consistent with this observation, the TG spectrum in Figure 5 exhibits a reduction in signal amplitude at $\omega_t = 16\,300$ cm^{-1} during this same time interval.

The calculated PE signals presented in Figure 9 capture the observed elongation of the PE spectrum at $T < 30$ fs in addition to a portion of the red-shift (50 cm^{-1}) in the ω_t dimension. The simulations predict that solvation causes relaxation in the shape of the PE spectrum (e.g., reduced elongation and red-shift in ω_t) at $T > 50$ fs, whereas the measurements in Figure 8 are dominated by dynamics at $T < 30$ fs. We believe that disagreement between the measured and simulated solvation time scales mostly likely reflects limitations of the spectroscopic model.[72] That is, solvation dynamics of CPC must possess an inertial component not accounted for by the model in Appendix B, which couples a single primary Brownian oscillator coordinate to each pigment excitation. In fact, evidence for an inertial solvation process was found in earlier studies of APC and α-phycocyanin.[25,30,76] Our PE measurements for APC and CPC suggest that the inertial solvent response is more prominent in CPC. This insight may be the key to understanding why exciton delocalization occurs in APC but not CPC.

The assignment of the dynamics in Figure 9 to nuclear relaxation should be addressed here because earlier experimental work found evidence of exciton electronic structure in the α84-β84 dimers of CPC.[30] A view of the system assuming exciton

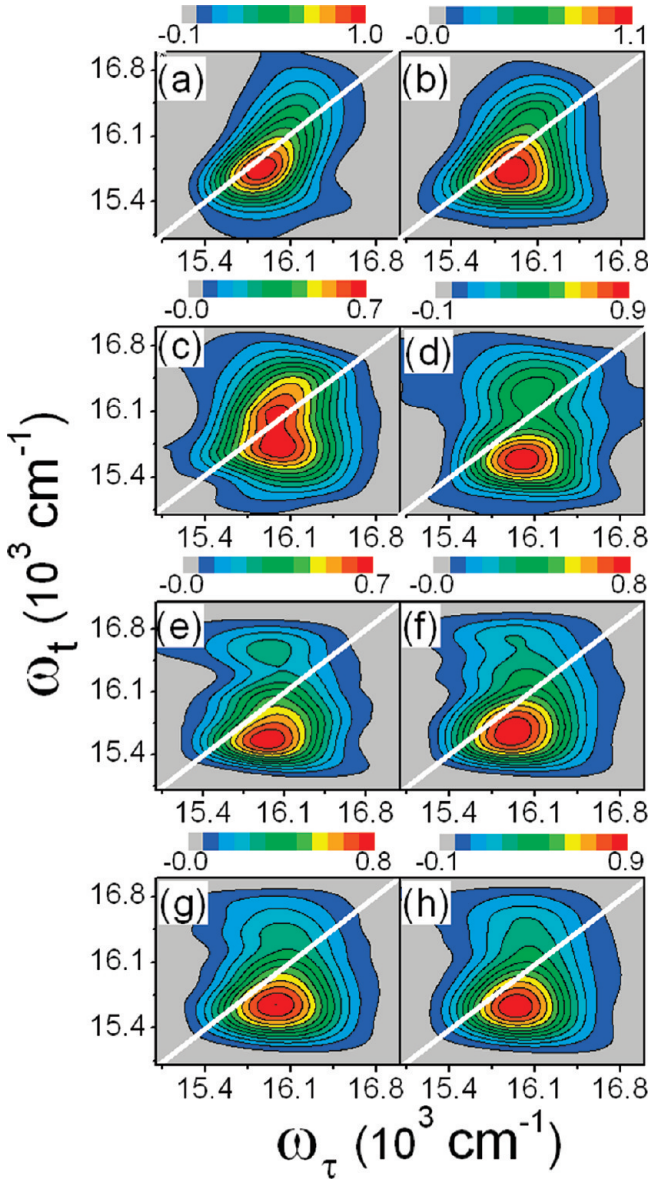

Figure 8. Real part of photon echo spectra measured at pulse delays, T: (a) 0 fs; (b) 10 fs; (c) 20 fs; (d) 30 fs; (e) 50 fs; (f) 70 fs; (g) 90 fs; (h) 120 fs. Pump (E_1 and E_3) and probe pulses (E_3 and E_4) are configured with magic angle polarizations. Amplitudes are scaled with respect to the peak signal amplitude at $T = 0$ fs. The contour lines in each panel are linearly spaced.

states could assign the rapid red shift of the 2D spectrum to internal conversion between exciton states. We address this issue by simulating the experiment using the exciton model outlined in Appendix C. The Hamiltonian assumes exciton formation within the α84-β84 dimers but neglects couplings (at zeroeth-order) between all other pairs of pigments. The approximations on which this model is based are consistent with experimental measurements as well as an analysis of interpigment interactions based on the X-ray crystal structure (see Appendix C).[28,29] The essence of the model is that the spectroscopic response can be decomposed into two independent systems: a two-level pigment (β155) and a dimer possessing four-level exciton electronic structure (α84 and β84). Figure 10a presents the energy level scheme, and Figure 10b shows a fit to the linear absorption spectrum obtained with the parameters described in Appendix C.

The calculated PE spectra in Figure 10c−10f clearly distinguish between predictions of the exciton model and experimental measurements. Excited state absorption (ESA) between the single

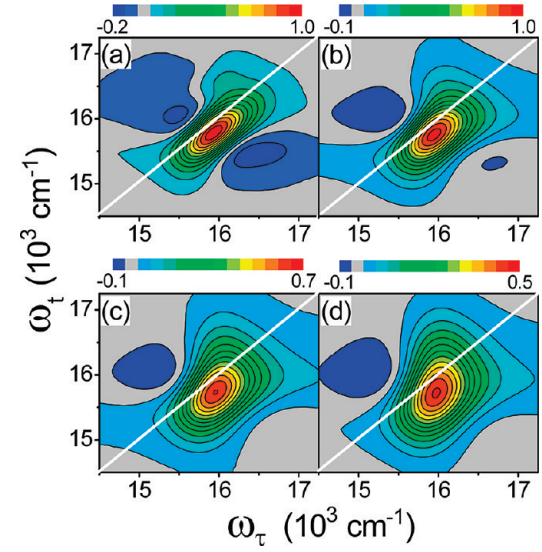

Figure 9. Real part of photon echo spectra calculated using parameters in Table 1 and equations in Appendix B where R1, R2, R3, and R4 are restricted to terms in which $a = b$. Pulse delays, T, are: (a) 0 fs; (b) 20 fs; (c) 50 fs; (d) 120 fs. Pump (E_1 and E_3) and probe pulses (E_3 and E_4) have magic angle polarizations. Amplitudes are scaled with respect to the spectrum at $T = 0$ fs. The contour lines in each panel are linearly spaced.

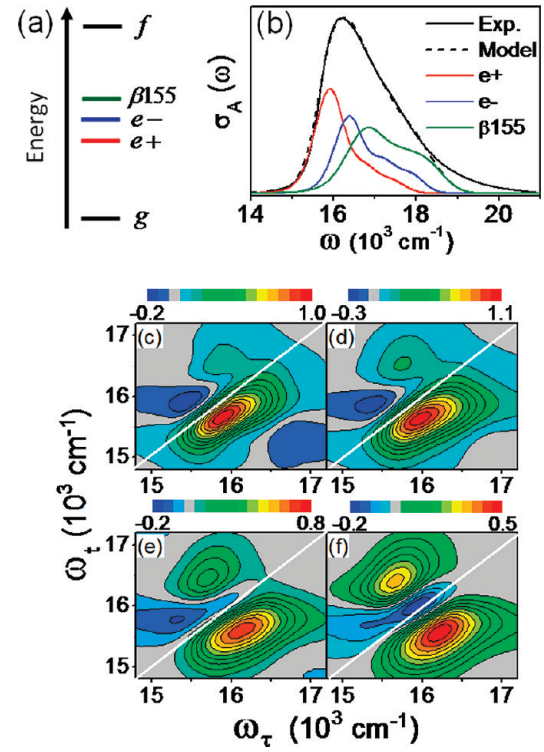

Figure 10. (a) Energy levels of the system in which exciton formation occurs between α84 and β84 pigments. (b) The absorption spectrum of CPC overlaid with the spectrum simulated using the parameters of Table 1. Calculated real part of photon echo spectra at pulse delays, T, are: (c) 0 fs; (d) 20 fs; (e) 50 fs; (f) 120 fs. The parameters in Table 1 and Equations in Appendix B are used where R1, R2, R3, and R4 are not restricted to terms in which $a = b$. Pump (E_1 and E_3) and probe pulses (E_3 and E_4) have magic angle polarizations.

exciton states, $e+$ and $e-$, and the double exciton state, f, produces interferences not found in our experimental data. It is even computed that the signal changes from positive to negative sign near $\omega_t = 16\,000$ cm^{-1}, whereas the sign of the measured signal is all-positive in this region. Furthermore, ESA produces interfer-

ences similar to those in Figure 10 for a wide range of input parameters. We regard these calculations as strong evidence against exciton formation in CPC. Of course, different ways of writing the exciton model can be envisioned.[31] However, we believe the present to be most plausible. Similar treatments of exciton electronic structure have successfully described the spectroscopic responses of other light harvesting proteins, including APC,[26] with strongly coupled pigments.[2,4,51,92] It should also be emphasizd that the line widths and transition dipoles involving the resonances between the single and double exciton states are constrained by fits of the linear absorption and fluorescence spectra (Figure 4), which are in fair agreement with those of Sauer and co-workers.[28,29] Therefore, we rule out the possibility that the ESA signal component discussed in Section IVC reflects exciton electronic structure; these nonlinearities are localized to the pigment sites and are unrelated to the double exciton state *f*.

V. Conclusions

The main conclusion of this paper is that electronic relaxation in the α84-*β*84 dimers of CPC proceeds by way of incoherent energy transfer. This conclusion is supported by comparing two different experimental measurements with the predictions of a theoretical model. (i) The anisotropy measurements and simulations presented in Figure 6 show that coherent cross terms in the response function give rise to a monotonically decaying anisotropy at $T <$ 100 fs. By contrast, our experimental data find that the sub-100 fs time scale is dominated by a 795 cm^{-1} recurrence corresponding to an impulsively excited HOOP vibration similar to that used by retinal to initiate signal transduction in vision.[55−58,93] The 60 fs dephasing time of this coherence is attributed to heterogeneity in the ground state (i.e., Franck−Condon) geometry of CPC rather than interexciton internal conversion. (ii) The measured PE line shapes in Figure 9 show no sign of the theoretically predicted interferences involving resonances between the single and double exciton levels depicted in Figure 10 (see also Appendix C). The presence of this higher-energy excited state, *f*, imposes strong constraints on an interpretation that assumes exciton electronic structure because the line shapes of spectroscopic transitions involving *f* derive from the same parameters that control the line shapes of absorption and fluorescence spectra (Figure 4). Similar exciton models successfully describe double exciton electronic structure of strongly coupled chromophores,[2,51,74,92] including APC.[26] Therefore, we believe the new information obtained in the present paper argues against exciton formation in CPC.

Insight into why CPC evolved with localized electronic states may be derived with consideration of its energy donor and acceptor pairs in the phycobilisome. CPC predominantly uses *β*155 to accept energy from phycoerythrin, which has a fluorescence maximum at 17 400 cm^{-1}. Extremely fast solvation in CPC apparently serves to ensure that energy transfer in the phycobilisome is unidirectional. First, energy transfer from CPC back to phycoerythrin is suppressed by solvation of the *β*155 pigment. Similarly, solvation of the α84-*β*84 dimer releases heat and suppresses energy transfer back to the *β*155 pigment. CPC is configured to direct energy to its α84-*β*84 dimer, where energy transfer to APC initiates. This paper suggests that inertial solvation processes are more prevalent in CPC than in APC and may be the key to understanding the different photophysics present in these two proteins.

Acknowledgment. Acknowledgment is made to the donors of the American Chemical Society Petroleum Research Fund for partial support of this research.

Appendix A. Calculation of Absorption and Fluorescence Spectra

Absorption and fluorescence spectra are calculated with

$$\sigma_{\mathrm{A}}(\omega) = \sum_{a=1}^{N} \mu_{ag}^2 \int_0^\infty \mathrm{d}t\{F_a^{00} + \sum_{\nu=1}^{2} F_{a\nu}^{01} \exp(-i\omega_\nu t)\} \times \exp\left[i(\omega - \omega_{ag})t - \frac{1}{2}g_{aa}(t)\right]\Phi_a(t) \quad \text{(A1)}$$

and

$$\sigma_{\mathrm{F}}(\omega) = \sum_{a=1}^{N} \mu_{ag}^2 P_a \int_0^\infty \mathrm{d}t\{F_a^{00} + \sum_{\nu=1}^{2} F_{a\nu}^{01} \exp(i\omega_\nu t)\} \times \exp\left[i(\omega - \omega_{ag})t - \frac{1}{2}g_{aa}^*(t)\right]\Phi_a(t) \quad \text{(A2)}$$

where N is the number of pigments; P_a is the Boltzmann factor representing the population of excited states; and $\Phi_a(t)$ accounts for lifetime broadening and is obtained by summing the Green function, $G_{ba}(t)$, over all population transfer channels as

$$\Phi_a(t) = \sum_b G_{ba}(t) \quad \text{(A3)}$$

Appendix B. Nonlinear Response Functions

This section summarizes expressions used to calculate transient grating and photon echo signals. This model is based on that presented in Sections 5.1 and 5.2 of ref 74. In ref 26, we modified the model for inclusion of vibronic structure. Here the equations are summarized to make clear how the parameters of Table 1 enter the calculation of nonlinear signals.

The six terms in the nonlinear response function are computed using

$$R_1(t_1,t_2,t_3) = \sum_{ab} \langle \alpha_{gb}\beta_{ag}\gamma_{bg}\chi_{ga}\rangle Z_{ab}^1(t_1,t_2,t_3)\exp\Big(-i\omega_{ag}t_1 - i\omega_{ab}t_2 - i\omega_{ag}t_3 - \frac{1}{2}f_1(t_1,t_1+t_2,t_1+t_2+t_3,0)\Big) \quad \text{(B1)}$$

$$R_2(t_1,t_2,t_3) = \sum_{ab} \langle \alpha_{gb}\beta_{ag}\gamma_{bg}\chi_{ga}\rangle Z_{ab}^2(t_1,t_2,t_3)\exp\Big(-i\omega_{gb}t_1 - i\omega_{ab}t_2 - i\omega_{ag}t_3 - \frac{1}{2}f_1(0,t_1+t_2,t_1+t_2+t_3,t_1)\Big) \quad \text{(B2)}$$

$$R_3(t_1,t_2,t_3) = \sum_{ab} \langle \alpha_{gb}\beta_{bg}\gamma_{ag}\chi_{ga}\rangle Z_{ab}^3(t_1,t_2,t_3)\exp\Big(-i\omega_{gb}t_1 - i\omega_{ag}t_3 - \frac{1}{2}f_1(0,t_1,t_1+t_2+t_3,t_1+t_2)\Big) \quad \text{(B3)}$$

$$R_4(t_1,t_2,t_3) = \sum_{ab} \langle \alpha_{ag}\beta_{ga}\gamma_{bg}\chi_{gb}\rangle Z_{ab}^4(t_1,t_2,t_3)\exp\Big(-i\omega_{ag}t_1 - i\omega_{bg}t_3 - \frac{1}{2}f_1(t_1+t_2+t_3,t_1+t_2,t_1,0)\Big) \quad \text{(B4)}$$

$$^{\mathrm{IC}}R_1(t_1,t_2,t_3) = \sum_{ab} \langle \alpha_{ga}\beta_{ag}\gamma_{bg}\chi_{gb}\rangle \exp[-i\omega_{ag}t_1 - i\omega_{bg}t_3 - g_{aa}(t_1) - g_{bb}(t_1) + 2i\lambda_{bb}t_3] \times Z_{ab}^{\mathrm{IC}}(t_1,t_3)[G_{ba}(t_2) - 1] - R_1(t_1,\infty,t_3) - R_4(t_1,\infty,t_3) \quad \text{(B5)}$$

$$^{IC}R_2(t_1,t_2,t_3) = \sum_{ab}\langle\alpha_{ga}\beta_{ag}\gamma_{bg}\chi_{gb}\rangle\exp[i\omega_{ag}t_1 - i\omega_{bg}t_3 - g^*_{aa}(t_1) - g^*_{bb}(t_1) + 2i\lambda_{bb}t_3] \times Z^{IC}_{ab}(-t_1,t_3)[G_{ba}(t_2) - 1] - R_2(t_1,\infty,t_3) - R_3(t_1,\infty,t_3) \quad (B6)$$

where the orientation part of the response function, $\langle\alpha_{ga}\beta_{ag}\gamma_{bg}\chi_{gb}\rangle$, is presented elsewhere (also in Supporting Information).[26,94,95] The $f_1(t_4,t_3,t_2,t_1)$ function is expanded according to

$$f_1(t_4,t_3,t_2,t_1) = g_{aa}(t_{21}) + g_{bb}(t_{43}) + g_{ab}(t_{32}) + g_{ab}(t_{41}) - g_{ab}(t_{31}) - g_{ab}(t_{42}) \quad (B7)$$

where $t_{ij} = t_i - t_j$ and the line broadening function is given by eq 2. The ad hoc auxiliary functions used to described vibronic couplings are

$$Z^1_{ab}(t_1,t_2,t_3) = F^{00}_a F^{00}_b + \sum_{\nu=1}^{2} F^{01}_{a\nu}F^{00}_b \exp[-(i\omega_\nu + k_\nu)(t_1 + t_2 + t_3)] + F^{00}_a F^{01}_{b\nu}\exp[(i\omega_\nu - k_\nu)t_2] + \delta_{ab}F^{01}_{a\nu}F^{00}_{b\nu}\exp(-i\omega_\nu t_1 - k_\nu(t_1 + t_2)) \times [\exp(-i\omega_\nu t_3) + (\exp(k_\nu t_2) - 1)] \quad (B8)$$

$$Z^2_{ab}(t_1,t_2,t_3) = F^{00}_a F^{00}_b + \sum_{\nu=1}^{2} F^{00}_a F^{01}_{b\nu}\exp[(i\omega_\nu - k_\nu)(t_1 + t_2)] + F^{01}_{a\nu}F^{00}_b \exp[-(i\omega_\nu + k_\nu)(t_2 + t_3)] + \delta_{ab}F^{01}_{a\nu}F^{00}_{b\nu}\exp(i\omega_\nu t_1 - k_\nu(t_1 + t_2)) \times [\exp(-i\omega_\nu t_3) + (\exp(k_\nu t_2) - 1)] \quad (B9)$$

$$Z^3_{ab}(t_1,t_2,t_3) = F^{00}_a F^{00}_b + \sum_{\nu=1}^{2} F^{00}_a F^{01}_{b\nu}\exp[i(\omega_\nu - k_\nu)t_1] + F^{01}_{a\nu}F^{00}_b \exp[-i(\omega_\nu + k_\nu)t_3] + \delta_{ab}F^{00}_a F^{01}_{a\nu}\exp[i(\omega_\nu - k_\nu)t_2] \quad (B10)$$

$$Z^4_{ab}(t_1,t_2,t_3) = F^{00}_a F^{00}_b + \sum_{\nu=1}^{2} F^{01}_{a\nu}F^{00}_b \exp[-i(\omega_\nu + k_\nu)t_1] + F^{00}_a F^{01}_{b\nu}\exp[-i(\omega_\nu + k_\nu)t_3] + \delta_{ab}F^{00}_a F^{01}_{a\nu}\exp[-i(\omega_\nu + k_\nu)t_2] \quad (B11)$$

$$Z^{IC}_{ab}(t_1,t_3) = F^{00}_a F^{00}_b + F^{00}_b \sum_{\nu=1}^{2} F^{01}_{a\nu}\exp(-i\omega_\nu t_1 - k_\nu|t_1|) + F^{00}_a \sum_{\nu=1}^{2} F^{01}_{b\nu}\exp(i\omega_\nu t_3 - k_\nu t_3) \quad (B12)$$

Appendix C. An Exciton Model For C-Phycocyanin

This section presents details on the Hamiltonian used to compute the photon echo signals in Figure 10. This exciton model adds interaction between the α84 and β84 pigments to the zeroeth-order Hamiltonian of eq 1 but neglects interactions between all other pairs of pigments. The neglect of couplings between pigments that are not members of the α84-β84 dimers can be motivated with the fluctuation amplitudes, Δ_{aa}, in Table 1. The assumption of localized electronic states holds when Δ_{aa} are large compared to intermolecular couplings which, with the exception of the dimer, are less than 75 cm^{-1}. Furthermore, the parameter, κ_a, indicates that the spectroscopic line widths are not motionally narrowed. Therefore, to a good approximation, heterogeneity in the site energies can be regarded as the source of wave function localization in CPC. This means that the parameters of Table 1 indicate the three α84 (or β84) pigments in the trimer (Figure 1) do not form a band structure as would be expected in a degenerate basis.[31] The present treatment is also consistent with the tens of picoseconds time scale for energy transfer involving pigments that are not members of the same dimer.[28,29]

The single exciton part of the Hamiltonian, $H1$, block diagonalizes as

$$H1 = \begin{pmatrix} E_{\beta 84} & J & 0 \\ J & E_{\alpha 84} & 0 \\ 0 & 0 & E_{\beta 155} \end{pmatrix} \quad (C1)$$

where subscripts are written on the diagonal elements to denote particular pigments and J represents coupling between the transition dipoles at the α84 and β84 sites. The energy level diagram in Figure 10a presents a notation for the three eigenstates obtained by diagonalization of $H1$: $e+$, $e-$, and β155.

The $e+$ and $e-$ states superpose excitations at α84 and β84. By the usual treatment of coupled two-level systems, Figure 10a also shows a doubly excited state, f, whose energy is given by the sum of $E_{\beta 84}$ and $E_{\alpha 84}$ (i.e., the double exciton Hamiltonian possesses a single element).

The exciton model is parametrized by setting the coupling, J, equal to -141 cm^{-1} and increasing the value of $\Delta_{aa}(\beta 84)$ from 510 to 610 cm^{-1}. The coupling strength, J, is consistent with earlier calculations based on the X-ray crystal structure of CPC.[28−30] Furthermore, we directly parametrize the exciton basis with the Franck−Condon factors in Table 1 by exchanging the β84 and α84 indices for $e+$ and $e-$. For example, the $F^{00}_a(\beta 84)$ and $F^{00}_a(\alpha 84)$ Franck−Condon factors of Table 1 become $F^{00}_a(e+)$ and $F^{00}_a(e-)$ in the present exciton model. Our treatment of Allophycocyanin similarly parametrizes Franck−Condon factors in the exciton basis.[26] All other parameters of Table 1 are unchanged. The present set of parameters fit the absorption spectrum quite well (Figure 10b) and suggest no need for further modification.

Diagonalization of $H1$ defines the rules needed to transform the line broadening functions of the β84 and α84 pigments (eq 2) from the local to the exciton basis.[2,4,74] The nonlinear response functions given in Appendix B still apply when supplemented with ESA terms (see Supporting Information).[2,26,74] The nonlinear response is restricted by allowing only the $e+$ and $e-$ states to radiate as coherent cross terms in which $a \neq b$. That is, the electronic states of β155 do not evolve in coherence with $e+$ and $e-$, which is again consistent with experimental work showing that its electronic relaxation occurs in the weak-coupling limit.[28,29] In other words, the four-wave mixing response of the present model essentially superposes nonlinearities of two independent systems: a two-level pigment (β155) and a four-level exciton dimer.

Supporting Information Available: Notation is given for the orientational part of the response function. Intramolecular reorganization energies of the phycocyanobilin pigments are estimated. Further explanation is given regarding correction of the chirp in the E_3 pulse for the measurement in Figure 5. This material is available free of charge via the Internet at http://pubs.acs.org.

References and Notes

(1) Capek, V.; Silinish, E. *Organic Molecular Crystals: Interaction, Localization, and Transport Phenomena*; AIP: New York, 1994.

(2) Abramavicius, D.; Palmieri, B.; Voronine, D. V.; Sanda, F.; Mukamel, S. *Chem. Rev.* **2009**, *109*, 2350.

(3) Fleming, G. R.; Scholes, G. D. *Nature* **2004**, *121*, 4221.

(4) Cho, M. *Chem. Rev.* **2008**, *108*, 1331.

(5) *Resonance Energy Transfer*; Andrews, D. L., Demidov, A. A., Eds.; Wiley: Chichester, 1999.

(6) Andrews, D. L. *Chem. Phys.* **1989**, *135*, 195.

(7) van Amerongen, H.; Valkunas, L.; van Grondelle, R. *Photosynthetic Excitons*; World Scientific: Singapore, 2000.

(8) Scholes, G. D. *Annu. Rev. Phys. Chem.* **2003**, *54*, 57.

(9) Davydov, A. *Theory of Molecular Excitons*; Plenum: New York, 1971.

(10) Mukamel, S.; Abramavicius, D.; Yang, L.; Zhuang, W.; Schweigert, I. V.; Voronine, D. V. *Acc. Chem. Res.* **2009**, *42*, 553.

(11) Zhuang, W.; Hayashi, T.; Mukamel, S. *Angew. Chem.* **2009**, *48*, 3750.

(12) Kimura, A.; Kakitani, T. *J. Phys. Chem. A* **2007**, *111*, 12042.

(13) Collini, E.; Scholes, G. D. *J. Phys. Chem. A* **2009**, *113*, 4223.

(14) Beljonne, D.; Curutchet, C.; Scholes, G. D.; Silbey, R. J. *J. Phys. Chem. B* **2009**, *113*, 6583.

(15) Sumi, H. *J. Phys. Chem. B* **1999**, *103*, 252.

(16) Jang, S.; Newton, M. D.; Silbey, R. J. *Phys. Rev. Lett.* **2004**, *92*, 218301.

(17) Scholes, G. D.; Jordanides, X. J.; Fleming, G. R. *J. Phys. Chem. B* **2001**, *105*, 1640.

(18) Schirmer, T.; Bode, W.; Huber, R.; Sidler, W.; Zuber, H. *J. Mol. Biol.* **1985**, *184*, 257.

(19) Schirmer, T.; Huber, R.; Schneider, M.; Bode, W.; Miller, M.; Hackert, M. L. *J. Mol. Biol.* **1986**, *188*, 651.

(20) Schirmer, T.; Bode, W.; Huber, R. *J. Mol. Biol.* **1987**, *196*, 677.

(21) Xie, X.; Due, M.; Mets, L.; Fleming, G. R. Femtosecond Fluorescence Depolarization Study of Photosynthetic Antenna Proteins: Observation of Ultrafast Energy Transfer in Trimeric C-phycocyanin and Allophycocyanin. *SPIE Symposium*, 1992.

(22) Edington, M. D.; Riter, R. E.; Beck, W. F. *J. Phys. Chem.* **1995**, *99*, 15699.

(23) Edington, M. D.; Riter, R. E.; Beck, W. F. *J. Phys. Chem. B* **1997**, *101*, 4473.

(24) Edington, M. D.; Riter, R. E.; Beck, W. F. *J. Phys. Chem B* **1996**, *100*, 14206.

(25) Homoelle, B. J.; Edington, M. D.; Diffey, W. M.; Beck, W. F. *J. Phys. Chem. B* **1998**, *102*, 3044.

(26) Womick, J. M.; Moran, A. M. *J. Phys. Chem. B* **2009**, in press.

(27) Gillbro, T.; Sharkov, A. V.; Kryukov, I. V.; Khoroshilov, E. V.; Kryukov, P. G.; Fischer, R.; Scheer, H. *Biochim. Biophys. Acta* **1993**, *1140*, 321.

(28) Debreczeny, M. P.; Sauer, K.; Zhou, J.; Bryant, D. A. *J. Phys. Chem.* **1995**, *99*, 8412.

(29) Debreczeny, M. P.; Sauer, K.; Zhou, J.; Bryant, D. A. *J. Phys. Chem.* **1995**, *99*, 8420.

(30) Riter, R. E.; Edington, M. D.; Beck, W. F. *J. Phys. Chem. B* **1997**, *101*, 2366.

(31) Zhang, J. M.; Zhao, F. L.; Zheng, X. G.; Wang, H. Z.; Yang, T.-S.; Hayashi, M.; Lin, S. H. *J. Photochem. Photobiol. B: Biol.* **1999**, *53*, 128.

(32) Kobayashi, T.; Baltuska, A. *Meas. Sci. Technol.* **2002**, *13*, 1671.

(33) Cerullo, G.; Nisoli, M.; De Silvestri, S. *Appl. Phys. Lett.* **1997**, *71*, 3616.

(34) Riedle, E.; Beutter, M.; Lochbrunner, S.; Piel, J.; Schenkl, S.; Spörlein, S.; Zinth, W. *Appl. Phys. B: Laser Opt.* **2000**, *71*, 457.

(35) Gallagher, S. M.; Albrecht, A. W.; Hybl, J. D.; Landin, B. L.; Rajaram, B.; Jonas, D. M. *J. Opt. Soc. Am. B* **1998**, *15*, 2338.

(36) Jonas, D. M. *Annu. Rev. Phys. Chem.* **2003**, *54*, 425.

(37) Maznev, A. A.; Nelson, K. A.; Rogers, J. A. *Opt. Lett.* **1998**, *23*, 1319.

(38) Goodno, G. D.; Dadusc, G.; Miller, R. J. D. *J. Opt. Soc. Am. B* **1998**, *15*, 1791.

(39) Cowan, M. L.; Ogilvie, J. P.; Miller, R. J. D. *Chem. Phys. Lett.* **2004**, *386*, 184.

(40) Brixner, T.; Mancal, T.; Stiopkin, I. V.; Fleming, G. R. *J. Chem. Phys.* **2004**, *121*, 4221.

(41) Pakoulev, A. V.; Rickard, M. A.; Meyer, K. A.; Kornau, K. M.; Mathew, N. A.; Thompson, D. E.; Wright, J. C. *J. Phys. Chem. A* **2006**, *110*, 3352.

(42) Mathew, N. A.; Yurs, L. A.; Block, S. B.; Pakoulev, A. V.; Kornau, K. M.; Wright, J. C. *J. Phys. Chem. A* **2009**, *113*, 9261.

(43) Strasfeld, D. B.; Shim, S.-H.; Zanni, M. T. *Adv. Chem. Phys.* **2009**, *141*, 1.

(44) Wright, J. C. *Int. Rev. Phys. Chem.* **2002**, *21*, 185.

(45) Gallagher Faeder, S. M.; Jonas, D. M. *J. Phys. Chem. A* **1999**, *103*, 10489.

(46) Hybl, J. D.; Albrecht Ferro, A.; Jonas, D. M. *J. Chem. Phys.* **2001**, *115*, 6606.

(47) Hybl, J. D.; Yu, A.; Farrow, D. A.; Jonas, D. M. *J. Phys. Chem A* **2002**, *106*, 7651.

(48) Khalil, M.; Demirdöven, N.; Tokmakoff, A. *J. Phys. Chem. A* **2003**, *107*, 5258.

(49) Asplund, M. C.; Zanni, M. T.; Hochstrasser, R. M. *Proc. Natl. Acad. Sci.* **2000**, *97*, 8219.

(50) Asbury, J.; Steinel, T.; Kwak, K.; Corcelli, S. A.; Lawrence, C. P.; Skinner, J. L.; Fayer, M. D. *J. Chem. Phys.* **2004**, *121*, 12431.

(51) Brixner, T.; Stenger, J.; Vaswani, H. M.; Cho, M.; Blankenship, R. E.; Fleming, G. R. *Nature* **2005**, *434*, 625.

(52) Read, E. L.; Engel, G. S.; Calhoun, T. R.; Mancal, T.; Ahn, T. K.; Blankenship, R. E.; Fleming, G. R. *Proc. Natl. Acad. Sci.* **2007**, *104*, 14203.

(53) Moran, A. M.; Dreyer, J.; Mukamel, S. *J. Chem. Phys.* **2003**, *118*, 1347.

(54) Zanni, M. T.; Ge, N. H.; Kim, Y. S.; Hochstrasser, R. M. *Proc. Natl. Acad. Sci.* **2001**, *98*, 11265.

(55) Andel, F., III; Murphy, J. T.; Haas, J. A.; McDowell, M. T.; van der Hoef, I.; Lugtenburg, J.; Lagarias, J. C.; Mathies, R. A. *Biochemistry* **2000**, *39*, 2667.

(56) Fodor, S. P.; Lagarias, J. C.; Mathies, R. A. *Biochemistry* **1990**, *29*, 11141.

(57) Lin, S. W.; Groesbeek, M.; van der Hoef, I.; Verdegem, P.; Lugtenburg, J.; Mathies, R. A. *J. Phys. Chem. B* **1998**, *102*, 2787.

(58) Palings, I.; Van den Berg, E. M. M.; Lugtenburg, J.; Mathies, R. A. *Biochemistry* **1989**, *28*, 1498.

(59) Womick, J. M.; Miller, S. A.; Moran, A. M. *J. Phys. Chem. B* **2009**, *113*, 6630.

(60) Womick, J. M.; Miller, S. A.; Moran, A. M. *J. Phys. Chem. A* **2009**, *113*, 6587.

(61) Miller, S. A.; Womick, J. M.; Parker, J. F.; Murray, R. W.; Moran, A. M. *J. Phys. Chem. C* **2009**, *113*, 9440.

(62) Goodno, G. D.; Astinov, V.; Miller, R. J. D. *J. Phys. Chem. B* **1999**, *103*, 603.

(63) Moran, A. M.; Nome, R. A.; Scherer, N. F. *J. Phys. Chem. A* **2006**, *110*, 10925.

(64) Moran, A. M.; Nome, R. A.; Scherer, N. F. *J. Chem. Phys.* **2007**, *127*, 184505:1.

(65) Milota, F.; Sperling, J.; Nemeth, A.; Kauffman, L. *J. Chem. Phys.* **2008**, *357*, 45.

(66) Lepetit, L.; Chériaux, G.; Joffre, M. *J. Opt. Soc. Am. B* **1995**, *12*, 2467.

(67) Tokunaga, E.; Terasaki, A.; Kobayashi, T. *J. Opt. Soc. Am. B* **1995**, *12*, 753.

(68) Khalil, M.; Demirdoven, N.; Tokmakoff, A. *Phys. Rev. Lett.* **2003**, *90*, 047401.

(69) Moran, A. M.; Maddox, J. B.; Hong, J. W.; Kim, J.; Nome, R. A.; Bazan, G. C.; Scherer, N. F. *J. Chem. Phys.* **2006**, *124*, 194904.

(70) Moran, A. M.; Park, S.; Scherer, N. F. *J. Phys. Chem. B* **2006**, *110*, 19771.

(71) Nakayama, T.; Amijima, Y.; Ibuki, K.; Hamanoue, K. *Rev. Sci. Instrum.* **1989**, *68*, 4364.

(72) Mukamel, S. *Principles of Nonlinear Optical Spectroscopy*; Oxford University Press: New York, 1995.

(73) Sundström, V.; Pullerits, T.; van Grondelle, R. *J. Phys. Chem. B* **1999**, *103*, 2327.

(74) Abramavicius, D.; Mukamel, S. *Chem. Rev.* **2004**, *104*, 2073.

(75) Brejc, K.; Ficner, R.; Huber, R.; Steinbacher, S. *J. Mol. Biol.* **1995**, *249*, 424.

(76) Riter, R. R.; Edington, M. D.; Beck, W. F. *J. Phys. Chem.* **1996**, *100*, 14198.

(77) Corcelli, S. A.; Lawrence, C. P.; Asbury, J. B.; Steinel, T.; Fayer, M. D.; Skinner, J. L. *J. Chem. Phys.* **2004**, *121*, 8897.

(78) Wang, C.; Stratt, R. M. *J. Chem. Phys.* **2007**, *127*, 224503.

(79) Elola, M. D.; Ladyani, B. M. *J. Chem. Phys.* **2007**, *126*, 084504.

(80) Harder, E.; Eaves, J. D.; Tokmakoff, A.; Berne, B. J. *Proc. Natl. Acad. Sci.* **2005**, *102*, 11611.

(81) Hayashi, T.; la Cour Jansen, T.; Zhuang, W.; Mukamel, S. *J. Phys. Chem. A* **2005**, *109*, 64.

(82) la Cour Jansen, T.; Knoester, J. *J. Chem. Phys.* **2006**, *124*, 044502.

(83) Moilanen, D. E.; Levinger, N. E.; Spry, D. B.; Fayer, M. D. *J. Am. Chem. Soc.* **2007**, *129*, 14311.

(84) Tokmakoff, A. *Science* **2007**, *317*, 54.

(85) Cowan, M. L.; Bruner, B. D.; Huse, N.; Dwyer, J. R.; Chugh, B.; Nibbering, E. T. J.; Elsaesser, T.; Miller, R. J. D. *Nature* **2005**, *434*, 199.

(86) Farrow, D. A.; Smith, E. R.; Qian, W.; Jonas, D. M. *J. Chem. Phys.* **2008**, *129*, 174509.

(87) Wynne, K.; Hochstrasser, R. M. *Chem. Phys.* **1993**, *171*, 179.

(88) Nagarajan, V.; Johnson, E. T.; Williams, J. C.; Parson, W. W. *J. Phys. Chem. B* **1999**, *103*, 2297.

(89) Parson, W. W. *Modern Optical Spectroscopy*; Springer-Verlag: Berlin, 2007.
(90) Qian, W.; Jonas, D. M. *J. Chem. Phys.* **2003**, *119*, 1611.
(91) Zhang, J. M.; Shiu, Y. J.; Hayashi, M.; Liang, K. K.; Chang, C. H.; Gulbinas, V.; Yang, C. M.; Yang, T.-S.; Wang, H. Z.; Chen, Y.-T.; Lin, S. H. *J. Phys. Chem. A* **2001**, *105*, 8878.
(92) Read, E. L.; Schlau-Cohen, G. S.; Engel, G. S.; Georgiou, T.; Papiz, M. Z.; Fleming, G. R. *J. Phys. Chem. B* **2009**, *113*, 6495.
(93) Kukura, P.; McCamant, D. W.; Yoon, S.; Wandschneider, D. B.; Mathies, R. A. *Science* **2005**, *310*, 1006.
(94) Hochstrasser, R. M. *Chem. Phys.* **2001**, *266*, 273.
(95) Dreyer, J.; Moran, A. M.; Mukamel, S. *Bull. Korean Chem. Soc.* **2003**, *24*, 1091.

JP908093X